Available online at www.sciencedirect.com
SCIENCE DIRECT
Thermochimica Acta 432 (2005) 177–185
thermochimica acta
www.elsevier.com/locate/tca

Non-adiabatic thin-film (chip) nanocalorimetry

A.A. Minakov [b,*], S.A. Adamovsky [a], C. Schick [a]

[a] *University of Rostock, Institute of Physics, Universitätsplatz 3, 18051 Rostock, Germany*
[b] *A.M. Prokhorov General Physics Institute, Vavilov 38, 119991 Moscow, Russia*

Received 7 November 2004; received in revised form 25 January 2005; accepted 31 January 2005
Available online 23 March 2005

Abstract

To study the kinetics of processes on a millisecond time scale a thin-film nanocalorimeter based on a commercially available microchip (thermal conductivity vacuum gauge, TCG 3880, from Xensor Integration, NL) was constructed. The gauge consists of a submicron silicon nitride membrane with a film-thermopile and a film-heater, which are located at the 100 μm × 100 μm central part of the membrane. Controlled fast cooling is possible in addition to fast heating at essentially non-adiabatic conditions. To allow fast cooling the measurements are performed in an ambient gas atmosphere. It is proved that the maximum rate of the controlled cooling can be achieved with a gas cooling agent, rather than in a system with a solid heat-sink. The advantage of the gauge TCG 3880 is that its central heated region is small enough to be considered as a point source of the heat-flow into the gas, which essentially simplifies the calorimeter calibration. The maximum cooling rate is inversely proportional to the radius of the heated region. The gauge is placed in a thermostat with controlled gas pressure and temperature to be utilized as a device for fast scanning calorimetry of sub microgram samples with sensitivity 1 nJ/K and time resolution ca. 5 ms.

Keywords: Ultra fast scanning calorimetry; Thin-film calorimetry; Nanocalorimetry; Melting and crystallization

1. Introduction

Ultra fast scanning nanocalorimetry is required to study kinetics of fast processes. It provides important information on thermodynamic properties and structure changes in materials at fast thermal treatments. This is of interest because a lot of modern materials are used in non-equilibrium states. The actual thermodynamic state of semicrystalline polymers, as an example, can be investigated only at sufficiently high heating rates ca. 10^3 K/s and even more [1–4]. Such rates are needed to prevent reorganization during the temperature scan. Only in this case it is possible to study exclusively the melting of the crystals originally present in the sample [5,6]. These non-equilibrium states are often generated by rapid cooling during material processing. Therefore, calorimetric experiments at high cooling rates comparable to processing conditions are required too. Thus, cooling rates up to 10^3 K/s are necessary for studies of phase transitions under the same conditions as during injection moulding of polymers [2–4]. The possibility of heat capacity measurements at high cooling rates is necessary for the investigation of crystallization and amorphization processes at quenching too.

Though heating rate can be enlarged by increasing heating power and decreasing sample mass [7–10], the only way to increase the cooling rate up to 10^3 K/s and larger is diminishing of the cell-sample dimensions, since the cooling possibility of any system is restricted by a finite heat transfer from the system. That is why a thin-film nanocalorimeter is very promising for fast cooling measurements. Obviously fast cooling measurements must be performed under essentially *non-adiabatic* conditions.

Thin-film calorimetry has been developed rapidly in recent years [7–16]. The major impulse is the general drive towards nanoscale objects in condensed matter physics. The capabilities of calorimetric techniques have been greatly enhanced with introduction of the silicon nitride membrane technology [16]. Constructing of a thin-film microchip module on

* Corresponding author. Tel.: +7 95 132 82 68; fax: +7 95 135 82 81.
E-mail address: minakov@nsc.gpi.ru (A.A. Minakov).

0040-6031/$ – see front matter © 2005 Elsevier B.V. All rights reserved.
doi:10.1016/j.tca.2005.01.073

a submicron silicon nitride membrane [17] therefore opens extensive capabilities. Sensitivity of such thin-film calorimeters can be very high primarily due to the very small addenda produced by the cell itself.

Recently Allen et al. developed a thin-film nanocalorimetry based on silicon nitride membranes for ultra fast heating, which was successfully applied for the study of numerous effects in a wide variety of nanosized samples [7–10,13–15]. The cell of the calorimeter consists of a thin-film heater deposited on a silicon nitride membrane. The heater simultaneously serves as a resistive thermometer. Thus, the heat capacity of ultra thin films [8,9] and separated polymer crystals [10], as well as nanoparticles and nanostructures [8,10] at ultra fast heating up to 10^5 K/s were investigated. Near-adiabatic conditions were achieved, when the cell was placed in vacuum ca. 10^{-5}–10^{-6} Pa. In the pioneering works custom designed sensors were constructed. At present, a number of commercially available microchip modules can be used as a sensor for thin-film nanocalorimetry [11,17–23].

In our study a commercially available thermal conductivity vacuum gauge TCG 3880 from Xensor Integration [17], which was applied for AC nanoscale calorimetry in [23], was used for non-adiabatic fast scanning calorimetry [5,6,22]. The measurements were performed in an ambient gas atmosphere rather than under adiabatic conditions to allow fast controlled cooling. Compared to specially designed calorimeter structures, the gauge TCG 3880 has significantly smaller active area (the heater size is about 50 μm × 100 μm), which presents a considerable advantage for non-adiabatic calorimetry [5,6,22]. Thus, the measurements at controlled heating and cooling rates up to 10^4 K/s were realized [5,6,22]. The kinetics of recrystallization and melt memory in semicrystalline poly(ethylene-terephthalate) (PET) on the time scales ranging from 5 ms to hours was investigated in previous papers [5,6]. As it was found for PET crystallized at 130 °C reorganization needs less than 40 ms between 150 and 200 °C. Additionally it was shown in [6] that isothermal reorganization of semicrystalline PET at 223 °C is about two orders of magnitude faster than isothermal crystallization from the isotropic melt at the same temperature.

The pressure gauge TCG 3880 is actually not optimized for fast scanning calorimetry. In the present work we therefore focused on basic aspects of non-adiabatic fast scanning calorimetry to allow the development of an even better sensor for fast scanning calorimetry. Finally, we present an improved experimental set-up of the thin-film (chip) nanocalorimeter.

To realize calorimetry at high scanning rates the addenda and the sample should have sufficiently small heat capacity. The cooling agent must be thermally “inertia less” too, i.e. it must have a small heat capacity as shown below. There are two possibilities to realize a fast cooling device: (i) using a solid heat sink (cold finger) made from high thermal conducting materials like metals but adding a large heat capacity to the system or (ii) using a low thermal conducting gas with very low heat capacity as the cooling medium. In order to make a decision which cooling medium is best suited for fast cooling we estimate the maximum cooling rate for both cases.

We assume at this point that the cooling system has no moving parts, i.e. no movement of the cooling agent occurs. In this case, as it is proved below, the highest cooling rate can be attained at the lowest heat capacity of the cooling agent, while the thermal conductivity is not a governing factor.

2. Upper limit of the scanning rate in fast cooling calorimetry

First, we determine the upper limit of the scanning rate for a system with a “cold finger” shown in Fig. 1.

A cell with a sample is placed at the flat face of a uniform rod with a specific heat capacity c, density ρ, thermal conductivity λ, and length L. The other face of the rod is coupled with a massive cooler, which is kept at a low temperature T_0. The temperature of the sample/rod interface is controlled by a thin flat heater with a negligible heat capacity and thermal resistance. Ideal thermal contacts between the sample and the heater, as well as between the heater and the rod, are assumed. To determine the upper limit of the scanning rate first suppose the heat capacities of the cell and the sample are small enough to be neglected. A uniform heat flux $q(t)$ is supplied to the face of the rod at $z = 0$ and transmitted along the rod axis. The heat leakage from the lateral surface of the rod is negligible. The temperature distribution in the rod $T(z, t)$ is described by Fourier’s heat-transfer equation:

$$\rho c \cdot \partial T(z,t)/\partial t = \lambda \cdot \partial^2 T(z,t)/\partial z^2. \quad (1)$$

Usually, the sample temperature is scanned linearly with time. Consider a saw-tooth shaped heating–cooling process with a period τ_0 and amplitude ΔT. The sample temperature is driven by a periodic heat flux $q(t)$ with an amplitude q_0 (the flux is changed in the range from 0 to $2q_0$). This periodic process can be presented as a sum of harmonic functions with pe-

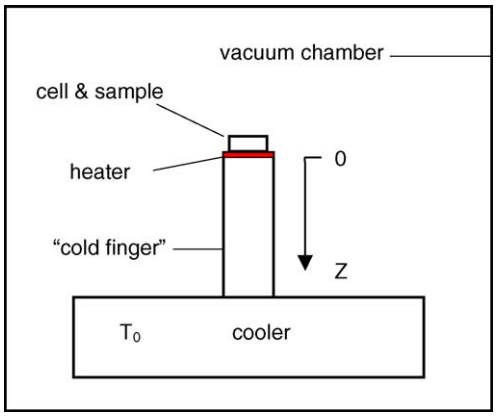

Fig. 1. Scheme of the system with a “cold finger”. The cell with the sample is placed at the flat face of a “cold finger” coupled with a cooler, which is kept at a low temperature T_0. The temperature of the sample is controlled by a thin heater located at the face of the finger.

riods $\tau_0/(2n+1)$ at $n = 0, 1, 2, \ldots$. According to Eq. (1) the amplitude of the temperature oscillation of the rod surface $z = 0$ at the frequency $\omega_0 = 2\pi/\tau_0$ equals $T_{A0} = q_{A0}/(\omega_0\rho c\lambda)^{1/2}$, provided the thermal length $l_0 = (2\lambda/\omega_0\rho c)^{1/2}$ is small with respect to L, where $q_{A0} \sim q_0$ is the heat flux amplitude at ω_0. The temperature of the rod surface is oscillating around the average value $T_{AV} = T_0 + T_B$, where the bias temperature T_B equals ca. $q_0 L/\lambda$. The amplitude of the temperature oscillations can be enhanced by varying the parameters in the relation $T_{A0} = q_{A0}/(\omega_0\rho c\lambda)^{1/2}$, but T_{A0} cannot be larger than T_B.

Generally, the parameter $c\rho$ does not depend essentially on the material chosen (except the low temperature region which is not considered at this point). In fact, $c\rho$ equals $(2 \pm 1) \times 10^6$ J/K m^3 at room temperature. To increase the amplitude T_{A0} at a fixed q_{A0} one can choose a material with a small thermal conductivity, but the choice is limited by the following restriction $\lambda \geq q_0 L/T_B^{max}$, where T_B^{max} is the largest acceptable temperature bias. For example, the minimal appropriate thermal conductivity λ equals 40 W/K m at the following predetermined parameters: $q_0 = 2 \times 10^5$ W/m^2 (20 W/cm^2), $L = 0.05$ m, and $T_B^{max} = 250$ K.

Next, the scanning rate can be estimated as the rate at the main harmonic: $\omega_0 \cdot T_{A0} \sim q_0 \cdot (\omega_0/\rho c\lambda)^{1/2}$. The rate increases with decreasing of τ_0. The minimal period τ_0 is limited by the smallest acceptable scanning amplitude ΔT^{min}, i.e. $q_0/(\omega_0\rho c\lambda)^{1/2} \geq \Delta T^{min}$. Therefore, the low limit for the scanning period is ca. $2\pi\rho c\lambda(\Delta T^{min})^2/q_0^2$, and for the optimal $\lambda = q_0 L/T_B^{max}$ it equals $\tau_0 \sim 2\pi\rho c L(\Delta T^{min})^2/q_0 T_B^{max}$. Finally, the maximal scanning rate $(dT/dt)_{max}$ can be estimated as the ratio of the peak-to-peak amplitude $2\Delta T^{min}$ and the time interval $\tau_0/2$:

$$(dT/dt)_{max} \sim (2q_0/\pi\rho c L) \cdot (T_B^{max}/\Delta T^{min}). \quad (2)$$

Consider the upper limit $(dT/dt)_{max}$ of the scanning rate at the following realistic parameters: $q_0 = 2 \times 10^5$ W/m^2, $L = 5$ cm, $T_B^{max} = 250$ K, $\Delta T^{min} = 50$ K. Then, $(dT/dt)_{max} \approx 6.3$ K/s and $\tau_0 \approx 32$ s for the rod of $c\rho = 2 \times 10^6$ J/K m^3 and $\lambda = 40$ W/K m. A further increase of the scanning rate at shorter scanning periods causes a decrease of the scanning range $2\Delta T$. For example, $(dT/dt)_{max} \approx 10$ K/s at $\Delta T^{min} = 30$ K, $\tau_0 \approx 11$ s. Generally, the product $\Delta T \cdot dT/dt$ is invariant with respect to the period τ_0. It can be estimated as the amplitude T_{A0} multiplied by the rate $\omega_0 \cdot T_{A0}$. Then, $\Delta T \cdot dT/dt \sim q_0^2/\rho c\lambda$ and for the optimal thermal conductivity $\lambda = q_0 L/T_B^{max}$ it equals:

$$\Delta T \cdot dT/dt \sim q_0 T_B^{max}/\rho c L. \quad (3)$$

Therefore, $\Delta T \cdot dT/dt \sim 500$ K^2/s at $q_0 = 2 \times 10^5$ W/m^2, $T_B^{max} = 250$ K, $c\rho = 2 \times 10^6$ J/K m^3 and $\lambda = 40$ W/K m. In fact, the value of this invariant is even smaller: $\Delta T \cdot dT/dt \approx 350$ K^2/s, as follows from an exact solution at the same parameters. The exact solution is further needed to make a quantitative discussion. Consider the exact solution for a semiinfinite rod. Note, that the thermal length

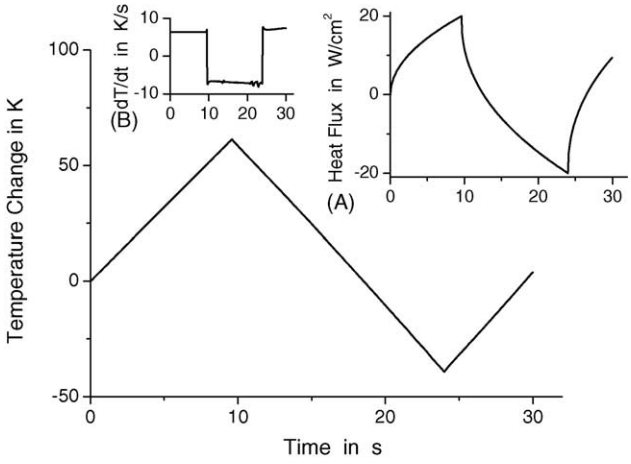

Fig. 2. Time dependence of the temperature change $T(0, t)$ on the surface of the rod at the heat flux $q(t)$ shown in the insert A. The temperature scanning rate is shown in the insert B.

$l_0 = (2\lambda/\omega_0\rho c)^{1/2}$ at the appropriate parameters is small enough with respect to L ($l_0/L \approx 0.28$ at $\tau_0 \approx 30$ s), that is the approximation of a semiinfinite rod is correct (analogous calculations can be easily performed for the opposite case $L < l$; in that case one has no advance in the scanning rate but has a smaller scanning interval).

The exact solution of Eq. (1) at the initial conditions $q(0) = 0$, $T(z, 0) = 0$ and the boundary condition $\partial T(z, t)/\partial z_{|z=0} = -q(t)/\lambda$ is as follows [24]:

$$T(z,t) = \sqrt{a/\pi} \cdot \int_0^t \exp[-(z^2/(4a(t-\tau)))] \cdot (q(\tau)/(\lambda\sqrt{t-\tau}))\,d\tau, \quad (4)$$

where $a = \lambda/\rho c$ is the thermal diffusivity of the rod. Consider the time dependency $T(0, t)$ of the temperature on the surface $z = 0$ at $c\rho = 2 \times 10^6$ J/K m^3 and $\lambda = 40$ W/K m. The heat flux should drive the temperature $T(0, t)$ linearly with time at cooling and heating. The required dependence $q(t)$ can be calculated exactly from the integral relation Eq. (4). To study limitations for the rate of the linear cooling one can use a simple model function $q(t)$:

$$q(t) = \begin{cases} q_0(t/0.8\tau_1)^{0.5} \\ \quad \text{at } 0 \leq t < 0.8\tau_1, \\ q(t) = q_0 - 2q_0[(t-0.8\tau_1)/1.2\tau_1]^{0.44} \\ \quad \text{at } 0.8\tau_1 \leq t < 2\tau_1, \\ q(t) = -q_0 + 2q_0[(t-2\tau_1)/\tau_1]^{0.44} \\ \quad \text{at } 2\tau_1 \leq t < 3\tau_1. \end{cases}$$

The function $q(t)$ provides an approximately liner dependence $T(0, t)$ (for one period) at heating and cooling, as shown in Fig. 2 for $\tau_1 = 12$ s and $q_0 = 2 \times 10^5$ W/m^2. The function $q(t)$ was constructed as follows. The heat flux $q(t) \sim \pm(t)^{1/2}$ provides almost linear temperature scanning in case of "inertia less" gas cooling agent [22]. When the cooling agent is a condensed matter the change of the heat flux should be faster

at the second step (at cooling) than at the first one (at first heating) because of the inertia of the rod. The model function $q(t)$ for the heating–cooling scan was found by the "trial and error" method.

The dependency shown in Fig. 2 illustrates the case of approximately linear cooling with the rate ca. 7 K/s, when the temperature changes from 61 to −39 K with respect to the reference level T_0. Thus the scanning range $2\Delta T \approx 100$ K corresponds to the time interval $\Delta t = 14.4$ s and $\Delta T \cdot dT/dt$ equals 350 K^2/s. The product $\Delta T \cdot dT/dt \approx 350$ K^2/s stays constant at different τ_1 as we proved numerically. The calculations are in good agreement with the previous estimation. The rate dT/dt still can be enlarged with decreasing the scanning interval, but it results in the reduction of the scanning range because the product $\Delta T \cdot dT/dt$ is invariant with respect to the scanning time interval.

In conclusion, we have found the limitation, ca. 10 K/s, for the maximal controlled cooling rate, which can be attained in a system with a "cold finger" at realistic parameters and the optimal thermal conductivity $\lambda = q_0 L / T_B^{max}$ (the optimal value λ can be reduced by diminishing L at the same q_0). The upper limit of the scanning rate $(dT/dt)_{max}$ is not determined by the thermal conductivity λ! Even the product $\Delta T \cdot dT/dt \sim q_0 T_B^{max}/\rho c L$ is determined only by the density and the specific heat capacity of the cooling agent. Thus, the parameter ρc should be reduced as much as possible to realize higher scanning rates. Consequently, the cooling agent must be a gas even at a low pressure, as long as the gas thermal conductivity stays reasonably large.

3. Non-adiabatic thin-film scanning calorimetry with a gas cooling agent

According to Eqs. (2) and (3) a gas is the best cooling agent for the fast scanning calorimetry. Also the addenda and the sample heat capacity should be as small as possible. Therefore thin-film calorimetry is required for fast scanning experiments. Consider the limitations for the scanning rate in the following two geometries. The first is a plate-like sample and the second is a point-like sample placed at a thin-film membrane, which serves as a heater and support. Suppose, the film-heater is very thin and it has negligibly small heat capacity. Also the heat transfer along the membrane is negligible.

In the first case, a thin-film sample of thickness d_s is deposited on the membrane. The film-system is placed in a gas with the following parameters: ρ_g, c_g and λ_g. The corresponding parameters of the sample are ρ_s, c_s and λ_s. The distance between the film and the thermostat wall L is small with respect the film lateral dimensions a and b. The temperature of the thermostat T_0 is kept constant. To estimate the upper limit of the cooling rate assume the distance L is small with respect to the thermal length in the gas $l_g = (\lambda_g \tau_0/\pi \rho_g c_g)^{1/2}$, which in the case of nitrogen gas at pressures in the range of 10^3–10^5 Pa equals ca. 2–25 mm at $\tau_0 = 1$ s ($\rho_g = 1.2$ kg/m^3, $c_g = 1.04$ J/g K, $\lambda_g = 0.026$ W/K m at room temperature and normal pressure [25]). Then, the heat flow from the sample into the wall equals $\Phi = \lambda_g ab(T - T_0)/L$, where T is the sample temperature (we neglect the heat transfer in the other directions). Note, that at increasing distance L the heat flow becomes smaller. In the case when $L > l_g$ the heat flow tends to $ab(T - T_0)(\pi \tau_0{}^{-1} \rho_g c_g \lambda_g)^{1/2}$.

The maximal cooling rate can be estimated from the relation $C \cdot dT/dt = \lambda_g ab(T - T_0)/L$, where the total heat capacity of the sample $C = abd_s \rho_s c_s$. The controlled cooling rate should be several times smaller than the estimated maximal possible rate $(dT/dt)_{max} = \lambda_g (T - T_0)/L d_s \rho_s c_s$. Thus, $(dT/dt)_{max}$ is ca. 7×10^3 K/s at $L = 100$ μm, $T - T_0 = 500$ K, $d_s = 10$ μm, $\rho_s c_s = 2 \times 10^6$ J/K m^3, and $\lambda_g = 0.026$ W/K m.

In the second case, consider a small disk-shaped sample of a thickness d_s and radius r_0 placed on a thin-film heater of the same radius located at the membrane centre. The distance from the heated region to the thermostat wall L and the thermal length in the gas l_g are large with respect to the radius r_0. Then at any relation between L and l_g, the heat-flow Φ from the point-like source of radius r_0 to the gas can be estimated as follows [5,6,22]: $\Phi = -4\pi r^2 \lambda_g dT_g(r)/dr$ at $r = r_0$, where the temperature in the gas around the heater equals $T_g(r) = T_0 + (T - T_0) r_0/r$. Consequently, the heat flow from the sample into the gas equals:

$$\Phi = (T - T_0) \cdot G, \tag{5}$$

where $G = 4\pi r_0 \lambda_g$ is the heat exchange parameter measured in W/K, which depends on the gas thermal conductivity. The parameter G equals ca. 2×10^{-5} W/K in air atmosphere at pressures in the range 10^3–10^5 Pa and room temperature [5,6,22] and it is ca. five times larger in helium gas. The measured value G is in agreement with Eq. (5) at $r_0 = 50$ μm. Then the maximal cooling rate in air can be estimated as $(dT/dt)_{max} \sim 4\lambda_g (T - T_0)/r_0 d_s \rho_s c_s$. Thus, $(dT/dt)_{max}$ is ca. 5×10^4 K/s at $r_0 = 50$ μm and the other parameters the same as in the first case.

The second case is the most promising. The rate $(dT/dt)_{max}$ can be even faster at smaller sample and heater dimensions. The shapes of the heated region and the sample do not have effect on the heat transfer into the gas, if the thermal length l_g is large with respect to r_0.

Another limitation on the scanning rate is related to the thermal gradient, which arises in the sample at fast scanning. If the maximal acceptable temperature difference across the sample equals δT_s, then the limiting rate is $(dT/dt)_{max} = \delta T_s \lambda_s / \rho_s c_s d_s^2$. Thus, for a polymer sample of a thickness $d_s = 10$ μm with $\rho_s c_s = 2 \times 10^6$ J/K m^3, and $\lambda_s = 0.3$ W/K m the rate $(dT/dt)_{max}$ equals ca. 5×10^3 K/s at $\delta T_s = 3$ K. The rate limit can be enlarged with diminishing of the thickness d_s. The limitation for the scanning rate due to the thermal gradient becomes equivalent to the former restriction at $d_s = r_0 \lambda_s \delta T_s / 4\lambda_g (T - T_0)$, i.e. at d_s ca. 1 μm for the same parameters as before.

Next, the temperature difference δT_c at the thermal contact between the sample and the heater should not be too

large. That is the thermal contact resistance must be sufficiently small. The maximal heat flux from the heater to the sample equals ca. $\rho_s c_s d_s (dT/dt)_{max}$. On the other hand, the heat flux through the contact is $q_c = R_c^{-1}\delta T_c$ by definition of the thermal contact conductance R_c^{-1} measured in W/m^2 K. Therefore, we can estimate $(dT/dt)_{max} \sim \delta T_c/\rho_s c_s d_s R_c$. Generally, the contact conductance measured between a dry joint of a polished surfaces equals ca. 2×10^3 W/m^2 K and it increases with contact pressure and temperature [26–28]. The thermal contact conductance becomes 10^2 times larger, if adhesive grease [29] is used to improve the contact. Generally the conductance R_c^{-1} can be 10^5–10^6 W/m^2 K for contacts with adhesive materials [29,30]. The adhesion between a polymer and the membrane becomes nice after first melting. Suppose the thermal contact conductance for the polymer/membrane interface is of the order of 10^5 W/m^2 K. Then, the limit of the scanning rate is ca. 2.5×10^4 K/s for $\delta T_s = 5$ K and the same parameters as in the previous section. However, at melting the apparent heat capacity can be of the order of 10^7 J/K m^3 (10 J/g K) [5,22]. In this case, the rate limit equals ca. 5×10^3 K/s. The effect of the thermal contact resistance can be reduced with decreasing sample thickness.

A further limitation on the scanning rate is imposed, when the film-sensor, which measures the temperature of the sample, is located on the membrane at a distance l_0 from the sample. This distance must be much smaller than the membrane thermal length $l_m = (\lambda_m/\pi\tau_0^{-1}\rho_m c_m)^{1/2}$, where ρ_m, c_m and λ_m are the corresponding membrane parameters, otherwise we have to consider thermal waves inside the membrane rather than a monotonous heating or cooling process. Therefore, the scanning period should be substantially large with respect to the characteristic delay time $\tau_m = \pi\rho_m c_m l_0^2/\lambda_m$. It equals ca. 5 ms at l_0 ca. 80 μm, the actual value for the gauge TCG 3880, and the following parameters $\rho_m = 3.4$ g/cm^3, $c_m = 0.17$ J/g K, $\lambda_m = 3$ W/K m for an amorphous silicone nitride membrane [31–33]. First the time resolution of the system is of the order of τ_m. Next, the scanning rate must be much smaller than $(T - T_0)/\tau_m \sim 8 \times 10^4$ K/s at $(T - T_0) = 500$ K [5].

Finally, consider the limitations on a controlled cooling rate for the gauge TCG 3880 placed in a gas. The sample temperature should be scanned approximately linearly with time, otherwise the calibration and the data evaluation becomes too complicated. Even if the maximum cooling rate in air can be 5×10^4 K/s, the controlled rate should be several times smaller than $(dT/dt)_{max}$. Generally, $C \cdot dT/dt = \Phi_0(t) - (T(t) - T_0) \cdot G$, where $\Phi_0(t)$ is the heat flow from the gauge heater [5,6,22]. The rate dT/dt can be controlled by the heater, provided $C \cdot dT/dt + (T(t) - T_0) \cdot G > 0$. Suppose, the cooling rate should be kept constant, i.e. $dT/dt = -|R_0|$. Then, during cooling the heat flow is reduced until $\Phi_0(t) = 0$ at $T(t) = T_0 + \Delta T_{min}$, where $\Delta T_{min} = |R_0|C/G$. At temperatures below $T_0 + \Delta T_{min}$ the cooling with the rate $-|R_0|$ cannot be controlled by the heater, which is switched off now. Consider the scan from T_0 to $T_0 + \Delta T$. The parameter ΔT_{min} should be several times smaller than ΔT, otherwise the temperature interval of the controlled cooling ($T_0 + \Delta T_{min}$, $T_0 + \Delta T$) will be too small for a practical use. In fact, the regions ca. few dozen of Kelvin at the ends of the scanning interval cannot be used for the data evaluation, because the scanning rate is changed from $+R_0$ to $-R_0$ and vice versa at the ends of the scanning interval. For example, the controlled cooling rate of the empty TCG 3880 cell should be several times smaller than $\Delta TG/C_0 \approx 5 \times 10^4$ K/s at $\Delta T = 500$ K, where C_0 is the addenda heat capacity ca. 2×10^{-7} J/K. This result is in agreement with the experiment. Therefore, the "controlled cooling rates up to 10^5 K/s" as discussed in [34] seems to be unrealistic high for real measurements with the gauge TCG 3880 placed in air. Also the modulation rate ca. 5×10^4 K/s realized in [23] should not be mixed with the scanning rate.

In conclusion, heat capacity measurements at a scanning rate up to 10^4 K/s can be realized in the thin-film calorimetry set-up utilizing the vacuum gauge TCG 3880. The heated region and the sample dimensions should be small with respect to other length scales of the sensor. Thermal gradients in the sample and on the thermal contact, even in the case of melting a polymer sample of a thickness ca. 10 μm, are in the order of a few Kelvin only for rates below 5×10^3 K/s.

4. Measuring cell

The thermal conductivity gauge TCG-3880 [17] shown in Fig. 3 consists of a sub micron amorphous silicon nitride membrane with a thin-film thermopile and a resistive film-heater located at the center of the membrane. All electrical connections are covered by an additional 0.7 μm SiO_2 layer for electrical insulation and protection. The six thermopile hot junctions—the white spots around the central region in the photograph—are arranged around the central heated area ca. 50 μm × 100 μm. The cold junctions are placed at the silicon frame fixing the membrane at a distance ca. 1 mm from the center. Thus the cold-junction temperature equals the temperature of the holder, which is close to the temperature of the thermostat. An additional copper–constantan thermocouple was utilized for the measurement of the holder temperature, which was used as the reference temperature T_0.

The silicone frame with the membrane is bonded to a standard chip carrier, as shown in Fig. 3. The distance from the membrane to the holder equals ca. 0.5 mm and to the thermostat wall ca. 10 mm. The whole assembly can be easily taken out of the thermostat and positioned under a microscope for sample handling. The gauge being installed in a thermostat with controlled temperature and gas pressure can be utilized as a sensor for fast scanning calorimetry of sub microgram samples.

The temperature measured by the thermopile does not represent the temperature of the heater/sample interface. The thermopile measures a temperature at the membrane around the heater at a distance ca. 50 μm from the heater perimeter. The measured temperature was calibrated as described

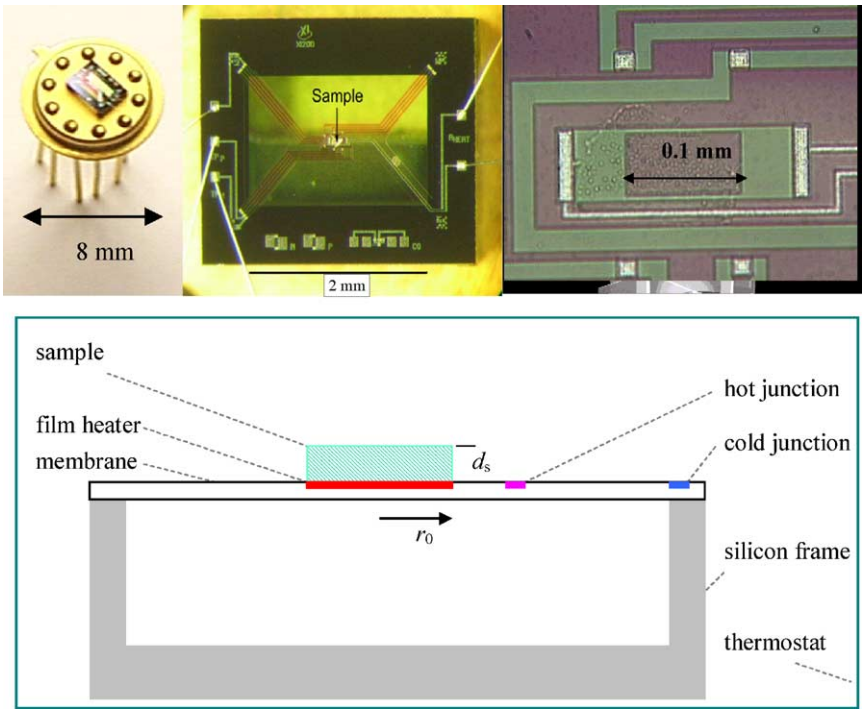

Fig. 3. Thermal conductivity gauge TCG-3880 utilized as a cell for the nanocalorimeter. And schematic cross-sectional view of the cell with a sample fixed at the middle of the membrane just at the film-heater.

in [22]. In the present work we analyze the temperature distribution $T(x, y)$ in the membrane plane around the heater. Consider the Cartesian axes with the origin O at the center of the membrane, axis Oz perpendicular to the membrane, axes Ox and Oy perpendicular to the sides of the rectangular heater in the membrane plane. We assume the scanning period is substantially large with respect to the characteristic delay time $\tau_m \approx 5$ ms in the membrane. To have a view of the temperature distribution in the membrane plane around the heater we determine the function $T(x, y)$ for the empty cell at steady-state heating.

In the case of a steady-state temperature distribution $T(x, y)$ the heat flow along the membrane plane into a volume increment $\Delta x \Delta y d_m$ equals $d_m \lambda_m (\partial^2 T/\partial x^2 + \partial^2 T/\partial y^2) \Delta x \Delta y$ and it is balanced by the heat flow from the surface $\Delta x \Delta y$ into the gas $\lambda_g \Delta x \Delta y (T - T_0)/L$, where d_m is the membrane thickness and L the distance from the membrane to the holder. Therefore, $\partial^2 T/\partial x^2 + \partial^2 T/\partial y^2 = k^2 (T - T_0)$, where $k^2 = \lambda_g/\lambda_m d_m L$. This is an equation with separable variables, that is $T(x, y) = T_0 + X(x)Y(y)$ and $(1/X)\,\mathrm{d}^2X/\mathrm{d}x^2 + (1/Y)\,\mathrm{d}^2Y/\mathrm{d}y^2 = k^2$. In fact, the distance from the central heated region to the membrane periphery is large with respect to the characteristic length $\sqrt{2}k^{-1} = (2\lambda_m d_m L/\lambda_g)^{1/2}$ which is ca. 0.24 mm at $d_m \approx 0.5$ μm, $L \approx 0.5$ mm, $\lambda_g = 0.026$ W/K m and $\lambda_m = 3$ W/K m. Therefore, the temperature drops down significantly with the distance from the heater, so that the boundary conditions at the membrane periphery are not essential. Consequently, in the case of the heat source located at the origin O the temperature distribution equals $T(x, y) = T_0 + (T^* - T_0) \exp(-k_x|x|) \exp(-k_y|y|)$, where T^* is the temperature at the centre and $k_x = k_y = k/\sqrt{2}$ for an isotropic membrane.

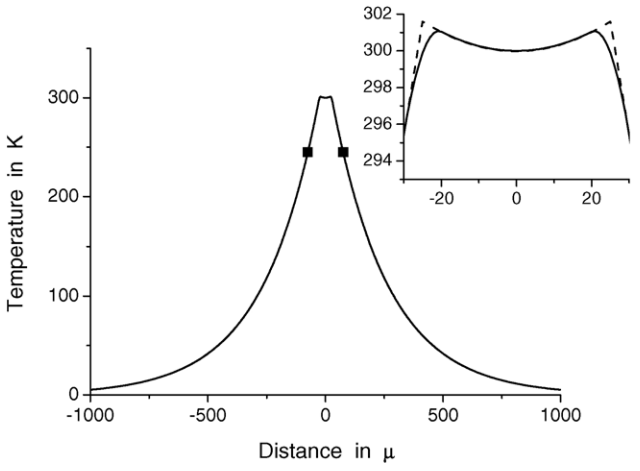

Fig. 4. Temperature $T(x, 0)$ vs. distance in the membrane plane along Ox axis at $T^* - T_0 = 300$ K. The square spots point to the measured temperature. The zoom of the central region is shown in the insert: the dashed curve was calculated for the infinitely thin heater and the solid line—for 5 μm width heater stripes.

In fact, the heater consists of two stripes oriented say along Oy axis and located at $x = \pm x_0$ with x_0 ca. 25 μm. Then, the dependence of the membrane temperature versus distance along Ox axis equals $T(x, 0) = T_0 + (T^* - T_0)\,[\exp(-k_x|x - x_0|) + \exp(-k_x|x + x_0|)]/2 \exp(-k_x x_0)$ at $y = 0$. The dependence is shown in Fig. 4. The temperature difference measured by the thermopile is ca. 80% of $T^* - T_0$

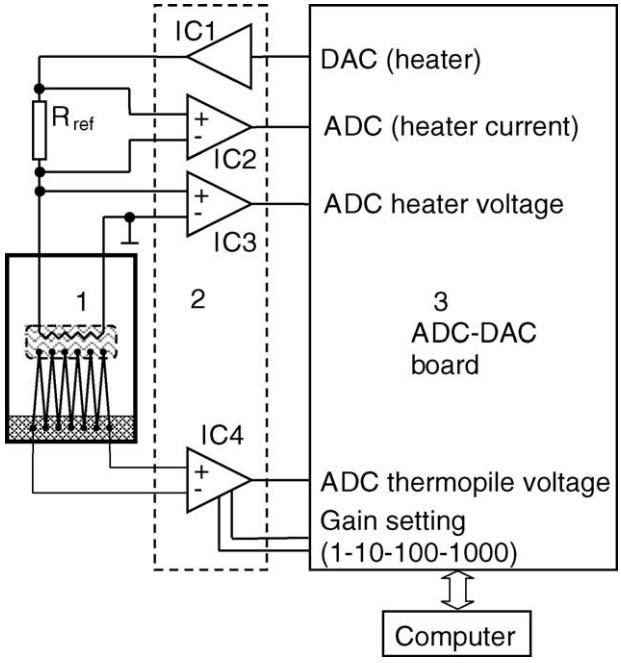

Fig. 5. Scheme of the calorimeter: 1—sensor; 2—amplifier; 3—ADC–DAC board. For details see text.

when the thermopile hot junctions are located at a distance 50 μm from the heater perimeter. The temperature difference $T(x, 0) - T_0$ at 1 mm from the membrane center is below 2% of $T^* - T_0$. Therefore, the boundary conditions at the membrane periphery are not important for the calculation of the temperature distribution around the heater.

Consider the temperature gradient inside the central heated area. First, we take into account that the heater stripes have a finite width. The dependence $T(x, 0)$ for the stripes of 5 μm width is shown in the insert of the Fig. 4. Inside the central heated region the temperature changes within 1 K at $T^* - T_0 = 300$ K, that is ca. 0.3% of $T^* - T_0$. Since a temperature gradient exists in the radial direction along the membrane, the sample should be placed just inside the central heated area. The sample size should ideally be such that it does not extend beyond the heater perimeter. Otherwise, there may be essential temperature gradient on the periphery of the sample outside the heated area.

5. Method: experimental details

The scheme of the calorimeter is shown in Fig. 5. The sensor (1) is connected through amplifiers (2) to the analog-to-digital and digital-to-analog converter (ADC–DAC) board (PCI-DAS64/M1/16 from Measurement-Computing™). A precision reference resistor R_{ref} (resistance of 100 Ω) is connected in series with the heater to measure the current through the heater. Data are collected at a rate of 5×10^4 samples/s. Two buffer differential amplifiers IC 2 and 3 (AD713J) are needed because the board requests low output impedance of the signal source if one wants to switch the inputs at high frequency. The preamplifier IC4 of type PGA204AP is used for the thermopile signal. The sensor is mounted to a cooper block, which is controlled at a fixed temperature T_0. The calorimeter can be filled or purged by dry nitrogen or helium even at reduced pressure if needed.

To achieve certain time-temperature profile the output voltage, which is fed to the heater through IC 1 (AD713J) at 5×10^4 samples/s, is calculated in advance as a function of time. Details of the procedure and the calibration of the device will be given elsewhere [35]. From the measured heater power and the thermopile signal heat capacity is derived as described below. Instrument control and data handling is realized by LabView™ program.

6. Method: calibration and data evaluation

The benefit of the gauge TCG 3880 is that its central heated region is small enough to be considered as a point source of a heat-flow in the gas. This heat-flow is proportional to the gas thermal conductivity λ_g and it can be easily estimated and calibrated. Furthermore, the smaller the heated region the larger the possible cooling rate. The resistive film-heater provides the heat flow $\Phi_0(t)$, which is supplied to the membrane/sample interface and propagates through the sample, the membrane and the ambient gas. The time dependence of the temperature of the membrane/sample interface is described by the following heat balance equation:

$$(C + C_0) \cdot \mathrm{d}T/\mathrm{d}t = \Phi_0(t) - (T(t) - T_0) \cdot G, \quad (6)$$

where C and C_0 are the heat capacities of the sample and addenda. The dependence $C_0(T)$ can be determined from the measurements for the empty cell. The addenda heat capacity $C_0(T)$ increases monotonously from 100 to 200 nJ/K in the temperature range 100–600 K and it equals ca. 150 nJ/K at room temperature [5,22]. The heat capacities of the film-heater and the film-thermopile are negligibly small. The main heat capacity of the cell is therefore the effective heat capacity of the heated part of the membrane. This equation is correct provided the thermal thickness of the sample is small enough, that is the rate $\mathrm{d}T/\mathrm{d}t$ does not exceed the acceptable maximum value discussed in Section 3.

There are two unknown parameters in Eq. (6)—G and C, at predetermined C_0. The heat transfer parameter G can be estimated according to the relation (5). Thus, at room temperature in air with $\lambda_g \approx 0.026$ W/K m the estimated value for G equals ca. 2×10^{-5} W/K, which was confirmed in the experiment [5,22]. The heat transfer through the gas is enlarged by a factor ca. 5, if helium gas is utilized. The effect of the membrane on the total heat exchange is relatively small (at least at gas pressures 10^3–10^5 Pa) because the membrane is very thin. The heat flow through the membrane in radial direction is ca. 50 times smaller than that through helium gas. The heat flow from the heated region due to radiation emission does not exceed 1–2% of the heat transfer though the gas

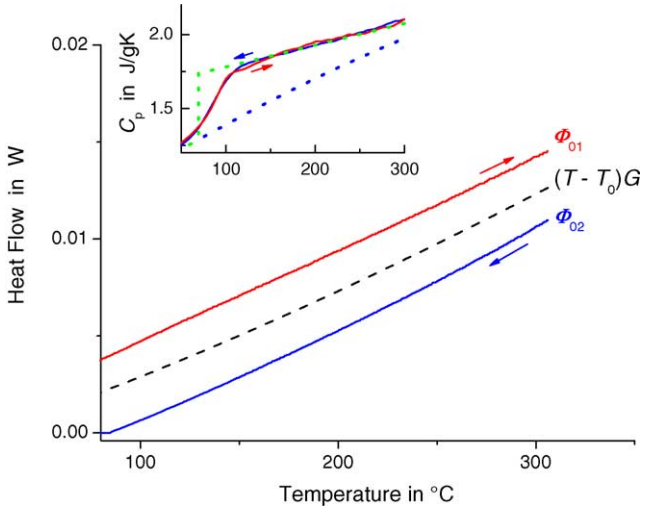

Fig. 6. Heat flow from the heater vs. temperature at heating and cooling (2×10^3 K/s) for amorphous PET sample ca. 480 ng—solid lines and heat flow into the gas—dashed line. The specific heat capacity $c_p(T)$ calculated according to Eq. (6) is shown in the insert. The dependences of $c_p(T)$ for completely amorphous and crystalline PET are given as provided by [37].

at $T = 600$ K and $T_0 = 300$ K, also the convective heat transfer in the small region ca. 100 μm is insignificant.

Thus, the temperature dependence of the heat exchange coefficient is mainly determined by the dependence $\lambda_g(T)$ and it can be approximated by a monotonous polynomial function [36]. The total value $G(T)$ can be calibrated in advance. Furthermore it can be measured simultaneously with the sample heat capacity from a heating–cooling scan as follows.

Suppose, we are interested in the dependence $C(T)$ of a sample near a phase transition temperature T_c, where heat capacity C_c at cooling is not the same as C_h at heating. Consider a heating–cooling scan in the range from $T_c - \Delta T$ to $T_c + \Delta T$, where ΔT is large enough to observe $C_c(T) = C_h(T)$ at least at the ends of the scanning interval far from T_c. Then the both functions $C(T)$ and $G(T)$ can be determined simultaneously as $C(T) = (1/2)[\Phi_{01}(t) - \Phi_{02}(t)]\cdot|dT/dt|^{-1} - C_0$ and $G(T) = (1/2)[\Phi_{01}(t) + \Phi_{02}(t)]\cdot(T(t) - T_0)^{-1}$ at temperatures far from T_c; $\Phi_{01}(t)$ and $\Phi_{02}(t)$ denote the heat flows at heating and at cooling respectively. Next, the monotonous function $G(T)$ is extrapolated into the phase transition region, where the sample heat capacities $C_c(T)$ and $C_h(T)$ can be determined finally as follows:

$$(C_h + C_0)\cdot|dT/dt| = \Phi_{01}(t) - (T(t) - T_0)\cdot G,$$
$$-(C_c + C_0)\cdot|dT/dt| = \Phi_{02}(t) - (T(t) - T_0)\cdot G. \quad (7)$$

Thus, the heat capacity of amorphous poly(ethylene terephthalate) (PET) sample ca. 480 ng was measured in air at 2×10^3 Pa and at the rate 2×10^3 K/s, see Fig. 6. The result was obtained from the heat flow temperature dependence at heating and cooling shown in Fig. 6. In order to determine the specific heat capacity, $c = C/m$, the sample mass m has to be known. The mass was not measured independently, because it was too small. It was determined from the measured heat capacity and the known $c_p(T)$ in the molten state at temperatures above T_c [37].

Further possibility is to measure heating–cooling cycle for a crystallized sample to investigate the melting. Then, just after the melting experiment one can measure the heating–cooling cycle for the amorphous sample obtained in the previous experiment. The dependence $G(T)$ determined in the second experiment can be used for the evaluation of the data of the melting experiment, provided the gas pressure was kept constant. Note the experiment usually lasts no longer than 1 s. Such experiment is illustrated in Fig. 7.

The melting curve $c_p(T)$ shown in Fig. 7 was obtained according to the heat-balance equation (7). The heat-exchange coefficient $G(T)$ was determined from the experiment with the amorphous sample after the melting experiment. Note, that the behavior of the semicrystalline sample near the glass transition drastically changes when the sample was cooled very fast (10^4 K/s) compared to the slow cooled (0.2 K/s) sample. The enthalpy relaxation peak in the glass transition region is very small after the quenching at 10^4 K/s. On the other hand, the pronounced enthalpy relaxation peak is observed above the glass transition after the relatively slow cooling. The enthalpy relaxation peak observed at the fast heating after the slow cooling is explained by the recovering of equilibrium in the non-equilibrium semicrystalline system [38].

The method described above was successfully applied to study melting and crystallization of linear polyethylene [22], PET [5,6], and submicron polyamide-6 (PA6) droplets in polystyrene/PA6 blends [39].

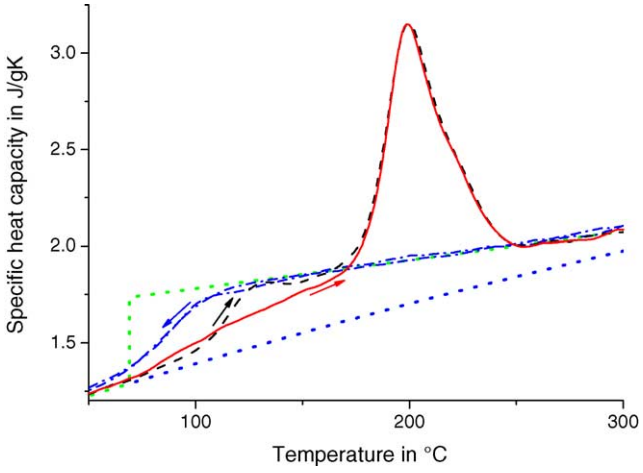

Fig. 7. Temperature dependence $c_p(T)$ for semicrystalline PET sample ca. 480 ng measured at 3×10^3 K/s after fast (10^4 K/s—solid line) and slow (0.2 K/s—dashed line) cooling-down below the glass transition temperature from the temperature of crystallization. The sample was crystallized for 15 min at 153 °C, and then cooled down to 30 °C. The dashed-dotted line represents the amorphous sample after the melting experiment. The curves for completely amorphous and crystalline PET (dotted lines) are shown according to [37].

7. Conclusions

In order to achieve the highest possible cooling rates for a calorimeter a gas cooling agent at reduced pressure is best suited because of the small value of $\rho_g c_g$ as shown in Section 3. The thermal conductivity λ_g is not the limiting factor for high cooling rates. Next, as shown further a small heater area, which can be considered as a point heater, allows about one order of magnitude faster cooling than a planar heater. The vacuum gauge TCG 3880 fulfils these conditions and was successfully utilized for fast scanning experiments on cooling and heating. The distance of ca. 50 μm between the heated area and the temperature sensor causes some problems, which must be considered for calibration. The results obtained can be used to design a better sensor for fast calorimetry.

Acknowledgements

The financial support of the German Science Foundation (DFG), grant numbers SCHI 331/7 and 436 RUS 17/108/01 is gratefully acknowledged.

References

[1] T.F.J. Pijpers, V.B.F. Mathot, B. Goderis, R.L. Scherrenberg, E.W. van der Vegte, Macromolecules 35 (2002) 3601.
[2] V. Brucato, F.G. Crippa, S. Piccarolo, G. Titomanlio, Polym. Eng. Sci. 31 (1991) 1411.
[3] Z. Ding, J.E. Spruiell, J. Polym. Sci. B: Polym. Phys. 34 (1996) 2783.
[4] V. Brucato, F. De Santis, A. Giannattasio, G. Lamberti, G. Titomanlio, Macromol. Symp. 185 (2002) 181.
[5] A.A. Minakov, D.A. Mordvintsev, C. Schick, Polymer 45 (2004) 3755.
[6] A.A. Minakov, D.A. Mordvintsev, C. Schick, Faraday Discuss, Self-Organizing Polymers 128 (2005) 270.
[7] S.L. Lai, G. Ramanath, L.H. Allen, P. Infante, Appl. Phys. Lett. 70 (1997) 43.
[8] M. Zhang, M.Y. Efremov, F. Schiettekatte, E.A. Olson, A.T. Kwan, S.L. Lai, T. Wisleder, J.E. Greene, L.H. Allen, Phys. Rev. B 62 (2000) 10548.
[9] M. Zhang, M.Y. Efremov, E.A. Olson, Z.S. Zhang, L.H. Allen, Appl. Phys. Lett. 81 (2002) 3801.
[10] A.T. Kwan, M.Y. Efremov, E.A. Olson, F. Schiettekatte, M. Zhang, P.H. Geil, L.H. Allen, J. Polym. Sci. B: Polym. Phys. 39 (2001) 1237.
[11] M. Jagle, Technisches Messen 70 (2003) 557.
[12] J.F. Mercure, R. Karmouch, Y. Anahory, S. Roorda, F. Schiettekatte, Physica B: Condensed Matter 340 (2003) 622.
[13] M.Y. Efremov, E.A. Olson, M. Zhang, Z.S. Zhang, L.H. Allen, Macromolecules 37 (2004) 4607.
[14] M.Y. Efremov, E.A. Olson, M. Zhang, S.L. Lai, F. Schiettekatte, Z.S. Zhang, L.H. Allen, Thermochim. Acta 412 (2004) 13.
[15] M.Y. Efremov, E.A. Olson, M. Zhang, F. Schiettekatte, Z.S. Zhang, L.H. Allen, Rev. Sci. Instrum. 75 (2004) 179.
[16] D.W. Denlinger, E.N. Abarra, K. Allen, P.W. Rooney, M.T. Messer, S.K. Watson, F. Hellman, Rev. Sci. Instrum. 65 (1994) 946.
[17] A.W. van Herwaarden, Thermochim. Acta, this issue. http://www.xensor.nl/pdffiles/tcg3880.pdf.
[18] J. Lerchner, A. Wolf, G. Wolf, J. Therm. Anal. Calorim. 57 (1999) 241.
[19] C. Auguet, J. Lerchner, P. Marinelli, F. Martorell, M.R. Rivera, V. Torra, G. Wolf, J. Therm. Anal. Calorim. 71 (2003) 951.
[20] W. Winter, G.W.H. Hohne, Thermochim. Acta 403 (2003) 43.
[21] J. Lerchner, R. Kirchner, J. Seidel, D. Waehlisch, G. Wolf, Thermochim. Acta 415 (2004) 27.
[22] S.A. Adamovsky, A.A. Minakov, C. Schick, Thermochim. Acta 403 (2003) 55.
[23] M. Merzlyakov, Thermochim. Acta 403 (2003) 65.
[24] I.N. Bronstein, K.A. Semendyayev, Handbook of Mathematics, 24th ed., Springer, Berlin, 2004, Chapter 1.13.2.
[25] D.R. Lid, Handbook on Chem. and Phys., 79th ed., CRC Press, 1998/1999, Chapters 4 and 6.
[26] S.M.S. Wahid, C.V. Madhusudana, Int. J. Heat Mass Transfer 46 (2003) 4139.
[27] V.V. Rao, K. Bapurao, J. Nagaraju, M.V. Krishna Murthy, Meas. Sci. Technol. 15 (2004) 275.
[28] A.J. Slifka, B.J. Filla, J.M. Phelps, J. Res. Natl. Inst. Stand. Technol. 103 (1998) 357.
[29] L.J. Salerno, P. Kittel, NASA Ames Research Center. http://irtek.arc.nasa.gov/CryoGroup/Archive/LS_98HB.word.
[30] Y. Xu, X. Luo, D.D.L. Chung, J. Electron. Packaging 124 (2002) 188.
[31] P.M. Sarro, A.W. van Herwaarden, M. Iodice, Thermophysical properties of low stress poly- and mono-silicon and silicon-nitride, in: Proceedings of the Conference Eurosensors VIII, Toulouse, France, 1994.
[32] B. Revaz, B.L. Zink, D. O'Neil, L. Hull, F. Hellman, Rev. Sci. Instrum. 74 (2003) 4389.
[33] http://www.ai.mit.edu/people/tk/tks/siliconnitride.html.
[34] M. Merzlyakov, Thermochim. Acta, submitted for publication.
[35] S. Adamovsky, C. Schick, in preparation.
[36] http://users.wpi.edu/∼ierardi/PDF/air_k_plot.PDF.
[37] B. Wunderlich, Pure Appl. Chem. 67 (1995) 1019–1026, http://web.utk.edu/∼athas/.
[38] Y.H. Jeong, I.K. Moon, Phys. Rev. B 52 (1995) 6381.
[39] R.T. Tol, A.A. Minakov, S.A. Adamovsky, G. Groeninckx, C. Schick, V.B.F. Mathot, in preparation.